Chinese Journal of
POLYMER SCIENCE

RESEARCH ARTICLE

https://doi.org/10.1007/s10118-023-2894-6
Chinese J. Polym. Sci. **2023**, *41*, 1093–1103

Robust Poly(glycolic acid) Films with Crystal Orientation and Reinforcement of Chain Entanglement Network

De-Yu Niu, Peng-Wu Xu, Si-Jie Xu, Jia-Xuan Li, Wei-Jun Yang, and Pi-Ming Ma*

The Key Laboratory of Synthetic and Biological Colloids, Ministry of Education, Jiangnan University, Wuxi 214122, China

Electronic Supplementary Information

Abstract The inherent brittleness of biodegradable poly(glycolic acid) (PGA) restricts its utilization in the packaging field. Traditional toughening methods usually require additional components accompanied by a sacrifice of strength. In the present work, PGA films with simultaneously enhanced strength and ductility are achieved *via* "casting-stretching-annealing" technology. The reinforced chain entanglement network of PGA induced by the intense extensional stress and the highly oriented crystals grown and refined during the stretching and annealing process endowed the improved ductility and strength of the PGA films, respectively. The relationships among the stretching process, microstructure and mechanical properties of the PGA films have been systematically investigated. As a result, the PGA film (SA-2) with low stretch ratios exhibits excellent ductility with an increase in elongation at break from 22% to 220% and tensile strength from 56 MPa to 130 MPa. Meanwhile, the PGA film (SA-4) with large stretch ratios features much higher tensile strength (335 MPa) while maintaining good ductility (elongation at break of 66%). In addition, highly oriented crystals result in obvious enhancement of heat resistance and dimensional stability of the PGA films. Therefore, this work provides an effective route to fabricate PGA films with both high strength and ductility which may promote the application of PGA materials.

Keywords Poly(glycolic acid); Uniaxial stretching; Ductility; Strength

Citation: Niu, D. Y.; Xu, P. W.; Xu, S. J.; Li, J. X.; Yang, W. J.; Ma, P. M. Robust poly(glycolic acid) films with crystal orientation and reinforcement of chain entanglement network. *Chinese J. Polym. Sci.* **2023**, *41*, 1093–1103.

INTRODUCTION

In recent years, many efforts have been attempted to address the environmental and ecosystem impacts caused by the overuse of plastic products.[1–3] The development and application of eco-friendly polymer materials is one of the promising solution strategies to tackle the plastic epidemic.[4,5] As a bio-compostable polyester, poly(glycolic acid) (PGA) possesses many advantages including great mechanical strength, chemical resistance and outstanding barrier properties, which make a great potential application in packaging.[6–9] However, the utilization scope of PGA is greatly restricted by its poor ductility.

Currently, the main strategies to achieve balanced mechanical performance of polymer are copolymerization and blending. Copolymerization can greatly improve toughness, thus many studies have focused on the synthesis and characterization of PGA copolymers such as poly(lactic acid-*co*-glycolic acid) and poly(glycolic acid-*co*-ε-caprolactone).[10,11] However, copolymerization often requires complicated design and synthesis processes, and sometime may have negative influence on other properties.[12] Another toughening method is melt-blending with flexible component, which is a more attractive and cost-effective strategy for industrial-scale production. Rubbers and flexible polymers were incorporated for toughening brittle polymers.[13–16] Specifically, in order to preserve biodegradability of PGA, the biodegradable polymers, such as poly(butylene adipate-*ran*-terephthalate) (PBAT)[17–20] and polycaprolactone (PCL),[21] were used primarily. Although good progress of PGA blends has been achieved for toughening PGA, several issues are yet to be addressed. (1) Most of the flexible component is immiscible with the polymer matrix and compatibilizers need to be introduced to obtain better toughening effect. As previously reported in our work,[19] the interfacial interaction and toughness were improved by the addition of epoxy functionalized copolymer. (2) The biodegradability and degradation ratio are hard to control when PBAT, PCL or compatibilizer is included in PGA matrix. (3) More importantly, the improved ductility in literature is usually accompanied by a sacrifice in mechanical strength. Therefore, it is still a challenge to simultaneously enhance the strength and ductility of PGA materials while maintaining good biodegradability.

Self-toughening techniques are gaining increasing attention, especially in polymer glass. The increased toughness caused by the mechanical rejuvenation of glassy polymers

* Corresponding author, E-mail: p.ma@jiangnan.edu.cn

Received September 22, 2022; Accepted October 28, 2022; Published online December 29, 2022

© Chinese Chemical Society
Institute of Chemistry, Chinese Academy of Sciences

(such as polycarbonate[22] and polystyrene[23,24]) has been confirmed and reasonably answered by a two-component model. The original two-component model decomposes interaction into covalent bonding in the chain network (primary bonds) and intersegmental van der Waals forces (secondary bonds).[25] Wang *et al.*[26,27] considered polymer glasses as a hybrid network formed by the nonbonded van der Waals force and the underlying load-bearing chain entanglement network. The ductile behavior resulting from mechanical rejuvenation and stretching is explained as an enhancement or densification of the load-bearing chain entanglement network.[28] Self-toughening technique is also applied to semi-crystalline polymers. For example, the enhanced toughness of poly(lactic acid) (PLA) by annealing[29,30] and high-temperature stretching[31–34] has been explored, which is attributed to a reduction in critical stress for shear yielding by robust chain entanglement network and high energy gauche-gauche (*gg*) conformers. In addition, stretch-induced orientation and crystallization are also effective in increasing strength.[35] In summary, finely constructing the crystalline and amorphous structure of semi-crystalline polymer is a feasible way to tailor the mechanical performance without any additional additives. However, to our best knowledge, the research on self-toughening or self-reinforcement of PGA is seldom reported.

PGA is difficult to be drawn at solid state due to its fast crystallization rate and high crystallinity, thus very brittle in general. In the present study, we obtained essentially amorphous PGA by quenching to allow ample space for manipulating the amorphous and crystalline structure. The oriented PGA crystals and the robust amorphous chain network were then induced by extensional stress and temperature fields. A scalable "casting-stretching-annealing" route is proposed in this work to fabricate PGA films with simultaneously improved strength and ductility. The oriented crystalline and lamellar structure are confirmed by X-ray scattering. Temperature-modulated differential scanning calorimetry (TMDSC) and dynamic mechanical analysis (DMA) are used to investigate the amorphous chain entanglement network. This study provides insight in the structural and property transitions upon the uniaxial stretching of PGA, which may develop a new approach for simultaneously enhancing strength and toughness of PGA products without additional additives.

EXPERIMENTAL

Materials

PGA pellets were kindly supplied by Shanghai Pujing Chemical Industry Co., Ltd., China. The number-average molecular weight and the polydispersity index are 1.7×10^5 g/mol and 1.3, respectively.

Sample Preparation

PGA was dried at 80 °C under vacuum overnight before processing. The PGA sheets with a low crystallinity and a thickness of 0.3 mm were made by casting process. Then, the PGA sheets were cut into squares of 90 mm × 90 mm, and uniaxially stretched to different stretch ratios (SRs) using a laboratory stretcher (HTU-200, Puliang Technology, Chain). Finally, the stretched PGA films were annealed at 130 °C. The fabrication process is shown in Fig. 1. For convenience, the films fabricated by casting-stretching and stretching-annealing process were abbreviated as CS-*x* and SA-*x*, where *x* indicates the SRs.

Characterization

Wide- and small-angle X-ray scattering (WAXS and SAXS)

The two-dimensional WAXS and SAXS measurements were performed on the XEUSS 3.0 bench equipped with a copper internal source (Genix3D) that produced an X-ray beam (λ=0.15418 nm) with an energy of 8 keV. The sample-to-detector distances were 60 and 500 mm for WAXS and SAXS measurements, respectively. All the acquisition time for measurements were set as 600 s. The 2D patterns were integrated to 1D intensity profile by software (XCACT) as function of scattering angle 2θ and scattering vector q ($q = 4\pi\sin\theta/\lambda$, where λ is the wavelength of the incident beam) for WAXS and SAXS measurements, respectively. The orientation parameter was measured by the Herman's orientation factor calculated by the following equations:

$$f_{hkl} = \frac{3\langle\cos^2\varphi_{hkl}\rangle - 1}{2} \tag{1}$$

$$\cos^2\varphi_{hkl} = \frac{\int_0^{\pi/2} I_{hkl}(\varphi)\cos^2\varphi\sin\varphi d\varphi}{\int_0^{\pi/2} I_{hkl}(\varphi)\sin\varphi d\varphi} \tag{2}$$

where φ is the azimuthal angle, $I_{hkl}(\varphi)$ is the azimuthal intensity distribution along (hkl) reflection of PGA. The inverse Fourier transform given as follows was applied to 1D-SAXS intensity profile $I(q)$ for obtaining the electron density correlation function $K(z)$ intensity:

$$K(z) = \frac{\int_0^{\infty} I(q)\, q^2\cos(qz)\, dq}{\int_0^{\infty} I(q)\, q^2 dq} \tag{3}$$

where z denotes the location measured parallel to the stretching direction, and $I(q)$ is the intensity. The long period (L), amorphous thickness (L_a) and lamellar thickness (L_c) structures

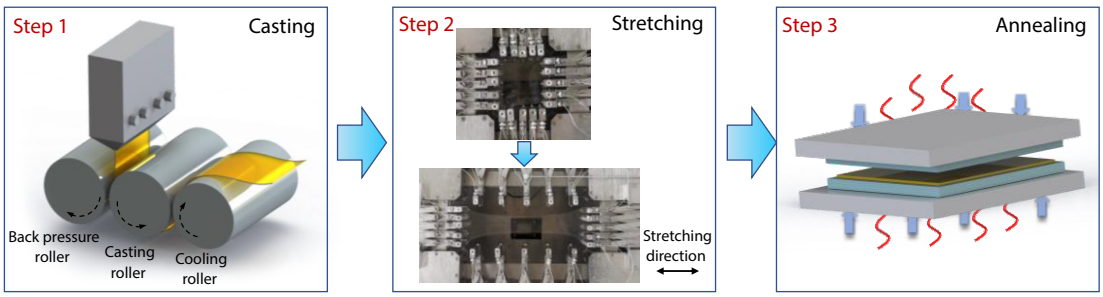

Fig. 1 Schematic diagram of the fabrication process of PGA films.

https://doi.org/10.1007/s10118-023-2894-6

can be obtained according to the previous method.[36] The smaller value was assigned as the average L_c, and the L_a can be calculated by $L_a = L - L_c$.

Temperature-modulated differential scanning calorimetry (TMDSC)

The DSC and temperature-modulated DSC (TMDSC) analysis of samples were studied with a Netzsch 204 F1 DSC instrument under nitrogen atmosphere (50 mL/min). Each sample (5 mg) was encapsulated in an aluminum closed pan. Samples were heated from 0 °C to 250 °C at a rate of 20 °C/min for DSC. In the TMDSC testing, the samples were heated from 20 °C to 70 °C at 3 °C/min with an oscillation period of 60 s and a temperature modulation amplitude of ±0.5 °C. The crystallinity ($X_{c,d}$) was calculated as follows:

$$X_{c,d} = \frac{\Delta H_m - \Delta H_{cc}}{\Delta H_m^0} \times 100\% \quad (4)$$

where ΔH_m^0 is the enthalpy of melting for 100% crystallinity of PGA (135 J/g).[9] The content of mobile amorphous fraction (X_{MAF}) and the rigid amorphous fraction (X_{RAF}) were calculated from the reversible heat capacity (C_p) in the glass transition region using the following equations:

$$X_{MAF} = \frac{\Delta C_p}{\Delta C_p^0} \quad (5)$$

$$X_{RAF} = 1 - X_{MAF} - X_{c,d} \quad (6)$$

where ΔC_p^0 is the heat capacity for totally amorphous PGA (0.642 $J \cdot g^{-1} \cdot {}^\circ C^{-1}$).[37]

Dynamic mechanical analysis (DMA)

DMA (Q800, TA instrument, USA) was used to characterize the thermal dynamic mechanical properties under a tensile-film mode. The test temperature was ranged from 20 °C to 90 °C, and the heating rate, frequency and amplitude were maintained as 3 °C/min, 1 Hz and 15 μm, respectively.

Mechanical properties

The tensile properties were measured according to GBT529-2008 standard by using a testing instrument (Instron5967, USA) with a tensile speed of 10 mm/min at room temperature and the results were the average of five independent specimens for each sample.

RESULTS AND DISCUSSION

Crystalline and Lamellar Structure of the Stretched PGA Films

Crystalline structural evolution of PGA films was explored by WAXS measurements. As shown in the 2D-WAXS patterns of PGA films in Fig. 2, only a diffuse halo scattering ring can be found in the CS films (SR from 1 to 4), reflecting very low crystallinity. It suggests that the crystallization is suppressed during casting process, and neither thermal nor stress induced crystallization occurs during stretching. It is reported that extensional stress could reduce nucleation barrier of critical nucleus to induce crystallization by forming ordered structures.[38] However, due to the low crystallization kinetics at stretching temperature (close to the T_g of PGA), no crystallization occurs during stretching. On the other hand, annealing could increase the crystallinity and crystalline perfection, thus all the SA films exhibit multiple scattering signals. The unstretched film (SA-1) displays isotropic typical scatting rings of PGA crystal, which can be indexed as (110) and (020) of PGA lattice planes. SA-2, SA-3, SA-4 films exhibit anisotropic scattering arcs. The scattering intensity of (110) and (020) reflections along the equator direction shows obvious reinforcement with increasing SRs. Meanwhile, a new scattering arc is observed in the meridian direction, which is assigned to the (002) of PGA lattice planes.[39] The corresponding 1D-WAXS curves are shown in Fig. 3(a). It is clearly seen that the CS films present a typical amorphous broad peak. After annealing, two strong scattering peaks are observed at 2θ=22.1° (110) and 28.6° (020). For evaluating the orientation of the crystalline in the SA films quantitatively, PGA (110) scatting was circularly integrated from 2D patterns to calculate orientation parameter (f) (see Fig. 3b and Fig. S1 in the electronic supplementary information, ESI). The f of SA-1 film is negligible (f=0.09) and then increases almost linearly to 5.4 as the SR increases to 4, indicating the formation of highly oriented PGA crystals.

The lamellar structure of PGA was further characterized by SAXS measurements. Fig. 4 illustrates the 2D-SAXS patterns of PGA films with different fabrication processes and SRs. Apparently, no visible scattering signal is observed in any CS films due to very low crystallinity, which is consistent with the

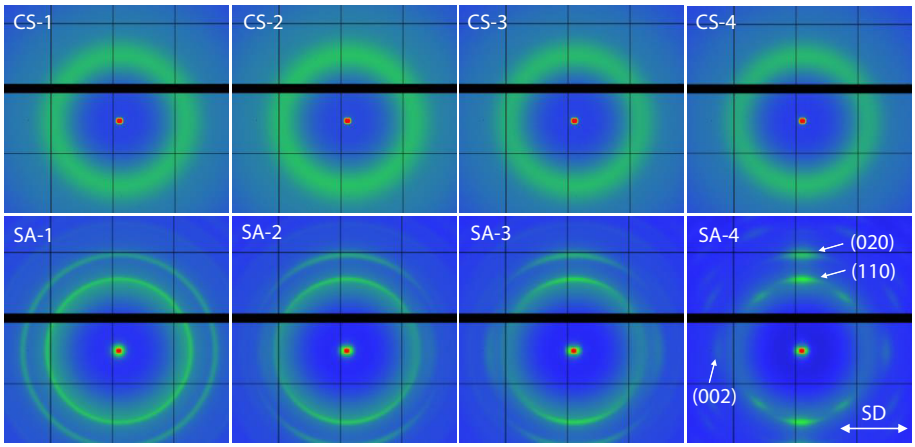

Fig. 2 Two-dimensional WAXS patterns of PGA films. The corresponding fabrication process and SRs are listed in the top left of each image. Stretching direction (SD) is shown by double-headed arrow.

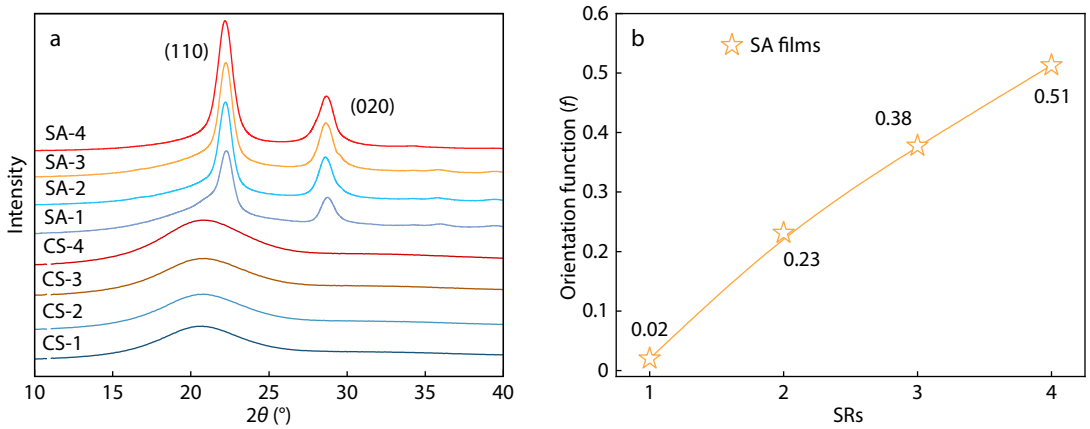

Fig. 3 (a) Representative 1D-WAXD patterns profiles (integrated along the equator direction) of PGA films; (b) Orientation parameter (*f*, associated with the PGA (110) reflection) of SA films as function of SRs.

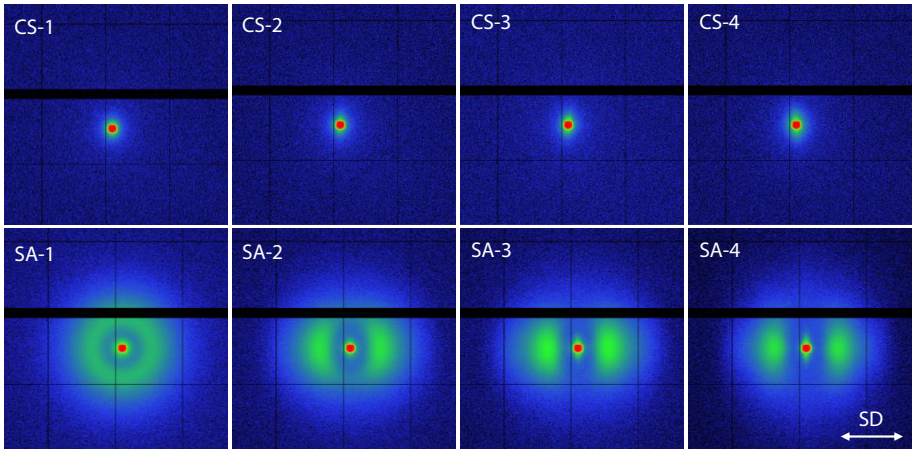

Fig. 4 Two-dimensional SAXS patterns of PGA films. The corresponding fabrication process and SRs are listed in the top left of each image. Stretching direction (SD) is shown by double-headed arrow.

WAXS results. In contrast, the formation of PGA crystals in SA films leads to a pronounced scattering signal in the 2D-SAXS patterns. The 2D-pattern of SA-1 film is circular of iso-intensity due to the initial random distribution of lamellar stacks. The scattered signals gradually concentrate into meridian with increasing SR, indicating the orientation of the lamellar. Moreover, the films with high SRs (CS-3, CS-4, SA-3 and SA-4) exhibit equator streak scattering across the beamstop, which indicates an elongated heterogeneous structure along the stretching direction such as microfibrils.[40] To obtain the detailed periodic information of the lamellae arrangement, the 1D-SAXS curves with Lorentz correction are integrated from 2D pattens along the meridian direction, as presented in Fig. 5(a). A scattering peak near q=0.8 nm^{-1} is observed in the annealed films (SA films). Long period (L), amorphous thickness (L_a) and lamellar thickness (L_c) of the SA films were calculated by Fourier transform correlation function, as summarized in Fig. 5(b). The L increases monotonically with increasing SR, which mainly stems from the crystalline thickening, as evidenced by the more noticeable increase in L_c and the essentially unchanged L_a. It is due to that the extensional stress-induced ordered molecular chains are more readily aligned into the lattice.[41]

Amorphous Architecture of the Stretched PGA Films

DSC and DMA were used to evaluate the amorphous structure of stretched PGA films that cannot be identified by X-rays. Fig. 6 shows the first DSC heating curves of CS and SA films and the thermal parameters are summarized in Table S1 (in ESI). For the CS films, DSC curves are characterized by glass transition, cold crystallization exotherm and melting endotherm. Two weak endothermic peaks are appearing near the glass transition temperature in the CS-3 and CS-4 films, which will be further discussed below in TMDSC results. The crystallinity of CS-1 film is 13.7% according to the Eq. (4) and increases to 20.7% of CS-4. It is not so consistent with the WAXS results in Fig. 2, which is probably attributed to the recrystallization and the lower enthalpy required for folding of locally ordered structure into lattice upon heating.[34,42] The gradual increase in crystallinity arises from stress-induced orientation and tiny crystallites, but it not yet detectable in X-rays. The orientation of amorphous molecular chains in the CS films is verified by the reduced cold crystallization temperature (T_{cc}) with increasing SR. The well-aligned amorphous chains could rearrange into lattice more easily, causing an earlier onset of cold crystallization.[43,44] In addition, the glass transition temperature (T_g) responds to the amorphous chain mobility. The damping factor (tanδ) curves in

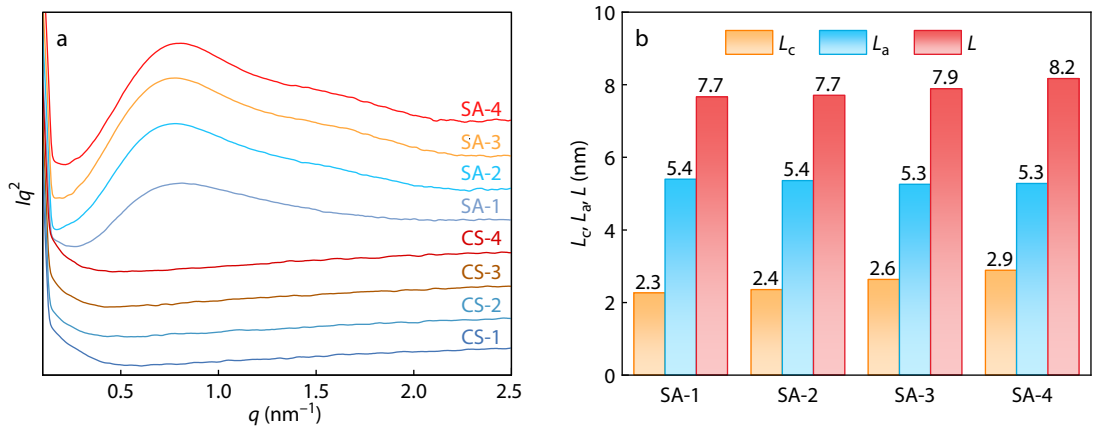

Fig. 5 (a) 1D-SAXS patterns profiles (integrated along the meridian direction) of PGA films; (b) Long period (L), amorphous thickness (L_a) and lamellar thickness (L_c) of the SA films as a function of SRs.

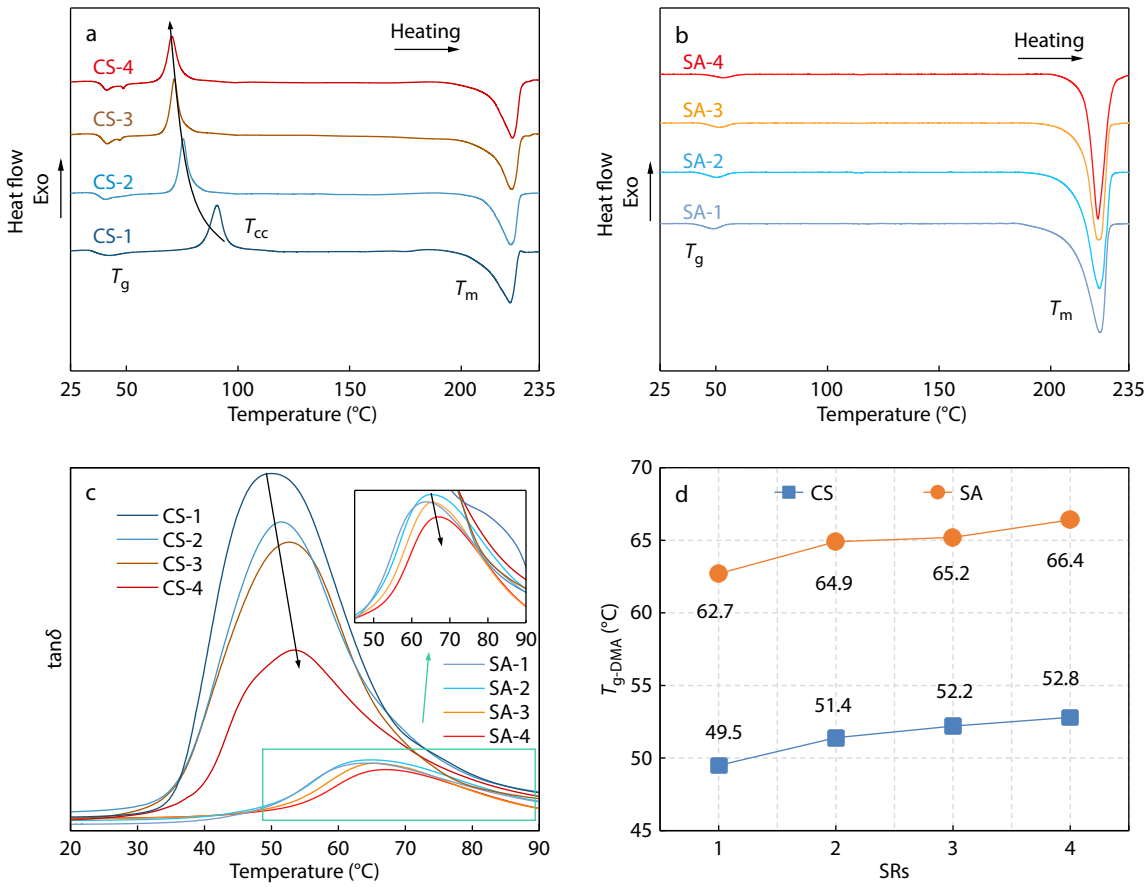

Fig. 6 DSC curves of (a) CS and (b) SA films with various SRs; (c) Temperature dependence of damping factor (tanδ) curves and the T_g of CS and SA films.

Fig. 6(c) clearly illustrates the T_g of PGA films and the corresponding values are presented in Fig. 6(d). The elevation in T_g from 49.5 °C for CS-1 to 52.8 °C for CS-4 indicated that the formation of ordered entanglement network suppresses the mobility and relaxation of PGA amorphous chains.[32,45] The reduction in tanδ_{max} with SR suggests a decrease of the relaxable molecular chain content.[46] After annealing, the SA films were crystallized with a crystallinity of round 50%, and the cold crystallization is absent in the DSC curves. The SA films exhibit larger increase in T_g compared to the CS films, because the refined PGA crystals further restrict the mobility of amorphous chains. It is worth noting that the T_g values of SA films increase from 62.7 °C to 66.4 °C as SR increases, although the SA films exhibit similar crystallinity, indicating that more ordered chain entanglement network in the stretched films.

TMDSC was used to further quantify and detect the ordered structure of the amorphous chains in the films. The nonreversible heat flow curves of CS films are shown in Fig.

7(a_1). Endothermic peaks and cold crystallization exothermic peaks are observed in the nonreversible heat flow of CS films. The endothermic peak is regarded as essentially the devitrification and relaxation of ordered molecular chain (*e.g.*, mesophase,[43] RAF,[47] or the physical aging[48]). Thus, the endothermic peak in this work is defined as chain relaxation peak. As SR increases, the chain relaxation temperature shifts to higher temperatures, while cold crystallization temperature gradually decreases. This is a clear evidence of the oriented amorphous chains formation during stretching. An interesting observation is that CS-3 and CS-4 films exhibit two chain relaxation peaks (around 37 and 43 °C, marked as T_1, T_2, respectively), indicating the presence of amorphous chains with different chain mobilities. The lower temperature peak is assigned to the relaxation of the less-hindered chains while the higher temperature peak corresponds to the devitrification of confined chains.[49] The reversible heat flow of the stretched films (Fig. 7a_2) exhibits an increase in T_g, accompanied by broader glass transition region and less amplitude. These findings also indicate that robust and ordered amorphous chain entanglement networks are created in the stretched films. The crystallinity (X_c), X_{MAF} and X_{RAF} of CS films are presented in Fig. 7(a_3). The X_{MAF} values are determined as 78 % of CS-1 and 50% of CS-4, which indicate that a large part of MAF chains is consumed and immobilized during the stretching process. Correspondingly, $X_{c\text{-PGA}}$ and X_{RAF} gradu-

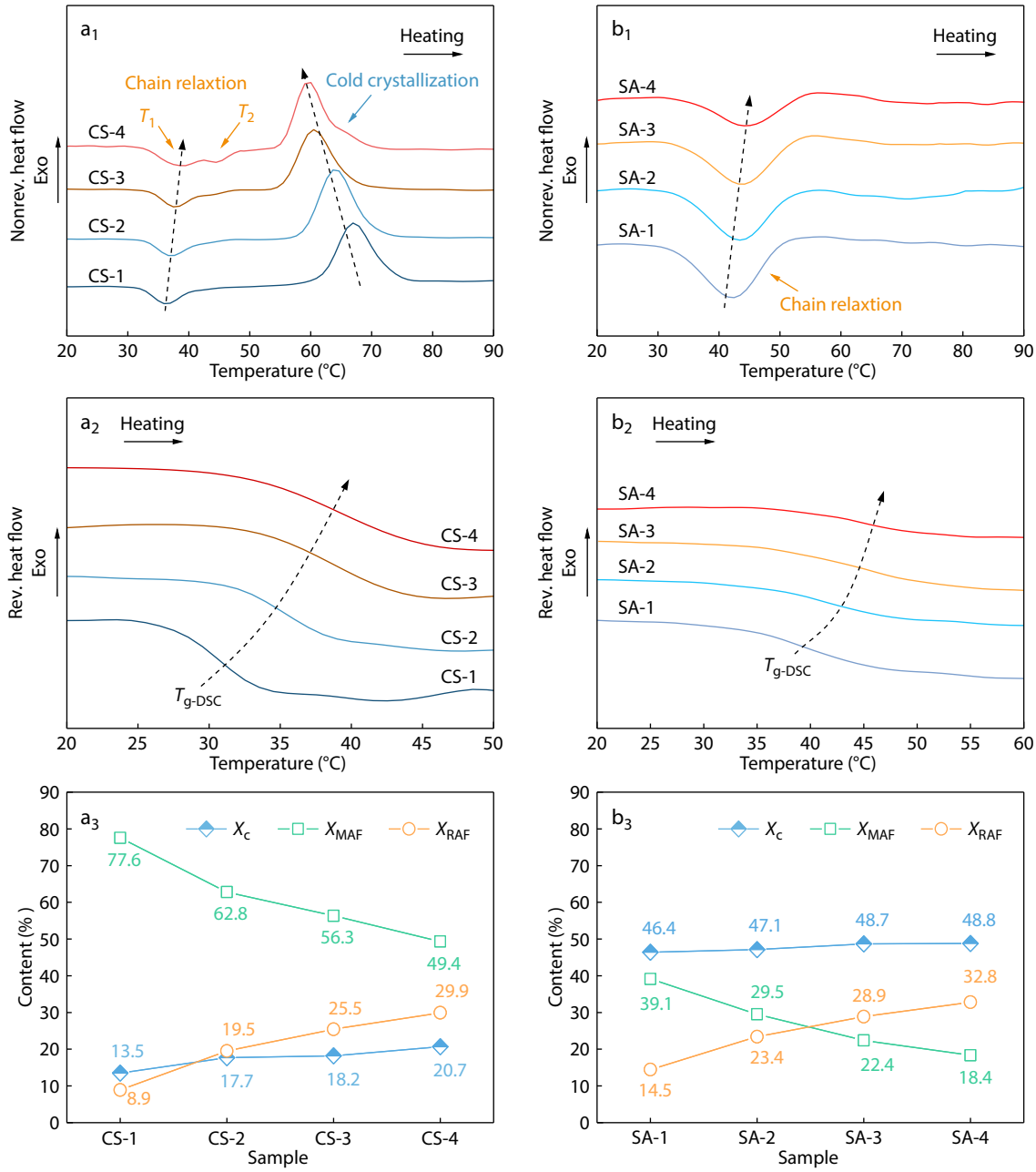

Fig. 7 TMDSC nonreversible heat flow curves (subscript 1), reversible heat flow curves (subscript 2), and the crystallinity (X_c), mobile amorphous fraction (X_{MAF}), rigid amorphous fraction (X_{RAF}) (subscript 3) for (a_1, a_2, a_3) the CS films and (b_1, b_2, b_3) the SA films.

https://doi.org/10.1007/s10118-023-2894-6

ally increase from 14% to 21% and from 20% to 30%, respectively. The high X_{RAF} value in CA-3 and CA-4 is probably responsible for the dual chain relaxation peak behavior in the nonreversible flow. The rigid amorphous chains need higher energy for relaxation during the glass transition process compared to the mobile amorphous chains, and thus exhibit higher chain relaxation peak (T_2). The TMDSC results of the SA films are presented in Figs. 7(b_1), 7(b_2) and 7(b_3). Attributed to the high crystallinity (about 50%), the relaxation of the amorphous chains including RAF and MAF is severely restricted by the crystallites. Thus, the SA films exhibit one chain relaxation peak and a glass transition region with less amplitude in the reversible flow. Moreover, the glass transition and chain relaxation of the SA films shift towards higher temperatures with SRs, suggesting that robust amorphous chain entanglement network is maintained during annealing process.

Mechanical and Heat-resistant Performance of the Stretched PGA Films

Mechanical properties

The mechanical properties of PGA films are presented in Fig. 8. As for CS films, the unstretched film (CS-1) exhibits high ductility

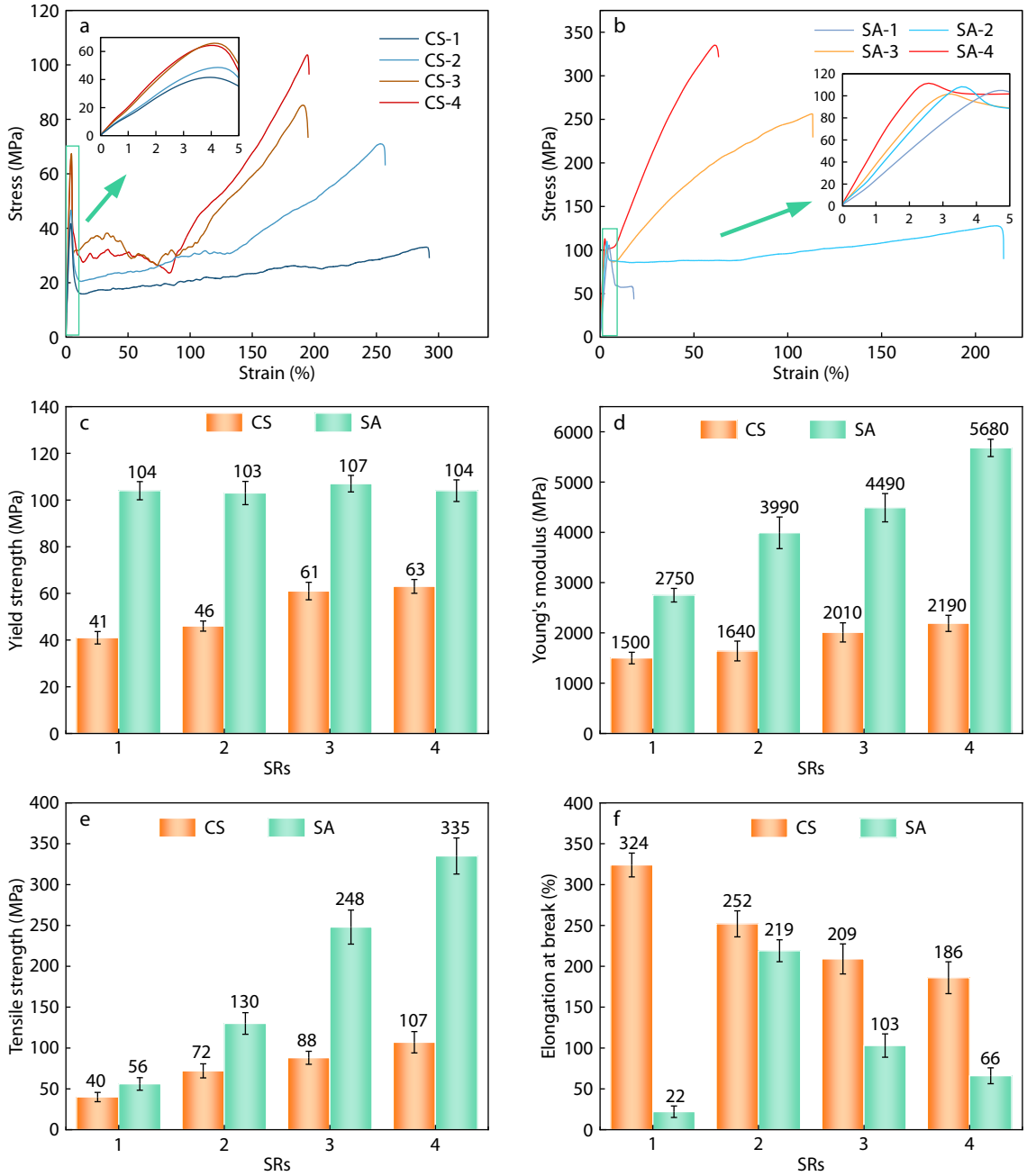

Fig. 8 The stress-strain curves of (a) CS and (b) SA films. Detailed mechanical properties of stretched PGA films including (c) yield strength, (d) Young's modulus, (e) tensile strength and (f) elongation at break.

https://doi.org/10.1007/s10118-023-2894-6

but modest strength. Uniaxial stretching has a positive effect on the strength and stiffness, as evidenced by the increase in the yield strength and Young's modulus to 63 and 2190 MPa, respectively, for CS-4 film. The significant strain hardening results in the markedly increase in tensile strength from 40 MPa to 72, 88 and 107 MPa with growing SR. After annealing, the yield strength of all SA films further increases to about 105 MPa. The effect of uniaxial stretching is reflected in the substantial improvement in the stiffness and ultimate tensile strength. The Young's modulus and tensile strength of SA-4 are as high as 5680 and 335 MPa, increased by 2.1 and 8.4 times relative to SA-1 films, respectively. Notably, the ductility of unstretched film drops significantly after annealing. In contrast, the stretched films maintain a high ductility after annealing. The elongation at break of SA-2 is identified as 220%, an increase of 188 % over SA-1.

Stretching above T_g could effectively improve the mechanical properties of semi-crystalline polymers by inducing the oriented amorphous molecular chains and crystallites with increasing X_c. As a result, the yield strength and modulus of CS films increase with growing SR, but the ductility decreases accordingly. After annealing, the increased PGA crystal orientation leads to an overall increase in the strength and modulus of SA films compared to CS films. Meanwhile, the crystallization during annealing consumes mobile amorphous chains and damages a part of chain entanglement, resulting in a noticeable reduction in elongation at break.[33,34] Interestingly, the orientation structure formed by stretching seems to maintain the amorphous chain entanglement network to some extent during annealing, which contributes to the ductility of the SA films. With further increase in SR, the highly oriented PGA crystals imparts an unexceptionable strength and modules of the films. Strain hardening is also a noteworthy factor in determining mechanical properties. A strong demonstration of stretch-induced amorphous chain orientation is the more obvious strain hardening as the SR increases. The more susceptible disorder-order transition of oriented amorphous chains is responsible for the early development and increased slope of strain hardening of stretched films.[32,36] In addition, the strain hardening of stretched films further moves to lower strain after annealing, accompanied by steeper slopes, suggesting that the more ordered structure in the annealed films shows strong molecular interactions during deformation. This is inconsistent with our usual assumption that heat-setting reduces the orientation. It is probably explained by the fact that the crystallization mainly consumes and immobilizes the mobile amorphous chains to form crystals, while the ordered rigid amorphous chains with higher cohesiveness are retained (as shown in Fig. 3). It also suggests that the pressure during annealing process could efficiently inhibit the relaxation of the oriented PGA chains.

Heat resistance and dimensional stability

The SA films with high crystallinity (as evidenced by WAXS and DSC results) are predicted to exhibit better dimensional stability than CS films at temperatures above T_g. DMA measurements and the deformation of film at 70 °C were used to prove this prediction more convincingly. Figs. 9(a) and 9(b) show the temperature dependence storage modulus (E') curves and the E' value at 70 °C of PGA films, respectively. As shown in Fig. 9(a), all the films exhibit a glass plateau region and a rubbery zone. The CS films show a sharp reduction in E' across glass transition region due to the lack of crystals. The E' then starts to increase as the temperature rises above 65 °C because of the cold crystallization. The E' at 70 °C of CS films are all lower than 500 MPa, indicating a poor heat resistance. In contrast, SA films exhibit a more modest decrease in E' at high temperatures compared to CS films. The E' at 70 °C of unstretched film increases from 94 MPa (CS-1) to 1401 MPa (SA-1). And it further increases to 2277 MPa (SA-4) with increasing SR owing to the crystalline orientation. Fig. S2 (in ESI) depicts the digital image of CS-4 and SA-4 before and after placing at 70 °C for 5 min, with the CS-1 as a comparison. The CS-4 and SA-4 films exhibit essentially the same length, indicating that the films did not shrink during annealing process. After 5 min at 70 °C, the CS-4 film shrinks completely to the same length as unstretched CS-1 film due to the relaxation of oriented PLA chains. In contrast, the SA-4 film shows almost no trace of shrinkage. These results confirm that the dense crystals formed during the annealing process can inhibit the deformation/relaxation of the amorphous regions, thus imparting a high modulus and good dimensional stability to the PGA films at such high temperatures.

Structural and Property Evolution of the Stretched PGA Films

PGA films with high strength, ductility and heat resistance were

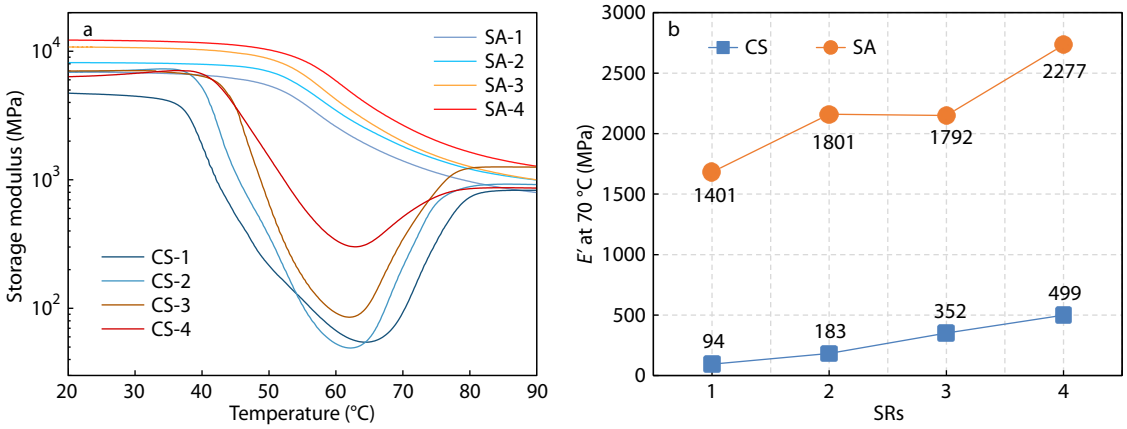

Fig. 9 (a) Temperature dependence of storage modulus (E') and (b) the value of E' at 70 °C for the PGA films.

https://doi.org/10.1007/s10118-023-2894-6

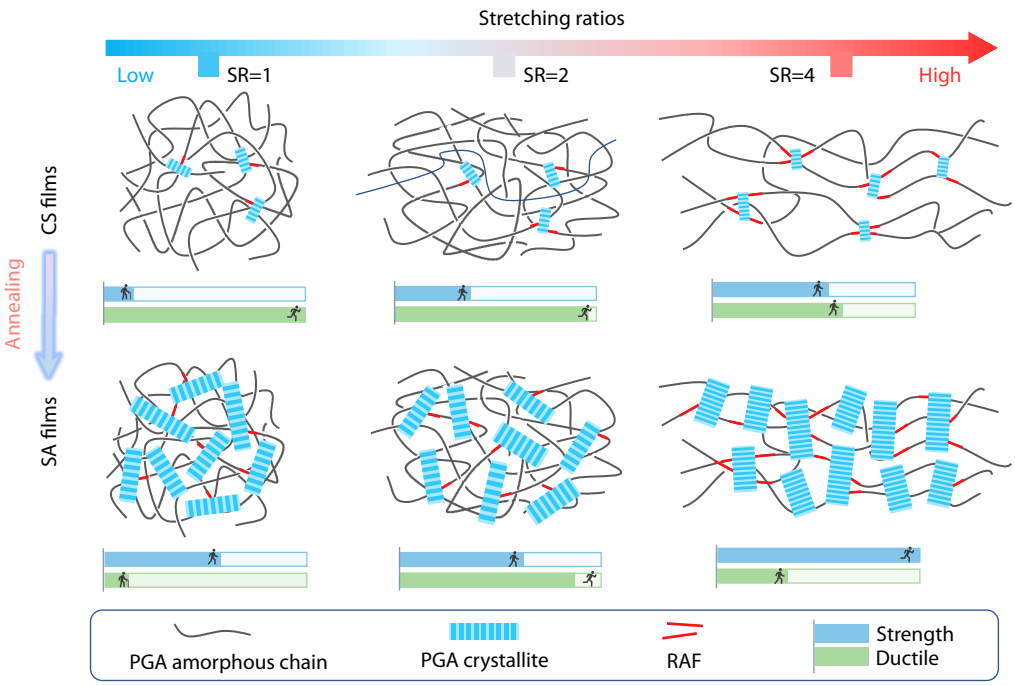

Fig. 10 Schematic representation of structural and property transmutation of PGA films with various SRs.

prepared by applying extensional stress and heat treatment. The superior comprehensive properties of PGA films are strongly related to the amorphous entanglement network and crystal structure. By combining X-ray scattering techniques, DSC, DMA and property characterization, we endeavor to illustrate the strengthening and toughening mechanisms of the stretched films as a guide for the design and fabrication of high-performance PGA materials. The schematic representation structural and property evolution of PGA films during stretching and annealing is illustrated in Fig. 10. The unstretched film (CS-1) is essentially amorphous with few crystallites and rigid amorphous chains. The film exhibits super-tough behavior but the strength and stiffness are extremely low. Uniaxial stretching provides a strong extensional stress to induce the orientation of PGA molecular chains and the formation of rigid amorphous chains, which construct a strong entanglement network in the amorphous regions. As SR increases, the CS films show more significant strain hardening and substantial increase in tensile strength. Meanwhile, no stress-induced crystallization occurs during stretching. The films possess good ductility due to the good mobility of the amorphous chains and lack of crystallite. After annealing, the formation of perfect PGA crystals provides more reinforcement elements, efficiently increasing the strength and stiffness of the PGA films. However, a sharp decrease in ductility is also observed because a large number of mobile amorphous chains are arranged into the lattice and thus destroying chain entanglement network. The stretch-induced ordered structure facilitates the maintenance of entanglement network and the improvement of ductility. Compared to the unstretched film (SA-1), a simultaneous improvement in strength and ductility is achieved in SA-2 due to the reinforced amorphous chain entanglement network and crystalline orientation. At high SR, the films possess an unexceptionable strength and good ductility due to the highly oriented PGA crystals and RAF. In addition, the physical cross-linking effect of the PGA crystals could restrict the deformation of the amorphous molecular chains, imparting great heat resistance and dimensional stability of the SA films.

CONCLUSIONS

Superior strong and tough PGA films were made by applying extension stress and heat treatment. The robust amorphous chain entanglement network is obtained during stretching process without stress-induced crystallization. The strength of stretched CS films is significantly improved, as well as a high-toughness behavior is achieved. Annealing process promotes the formation of oriented crystals in the stretched films, leading to a further substantial increase in strength and stiffness. The stress-induced ordered structure could preserve the chain entanglement network during annealing to a certain extent. The tensile strength and elongation at break of annealed SA-2 film are 130 MPa and 220%, respectively, which are 130% and 900% higher than those of SA-1 film. The tensile strength is further enhanced to an impressive 335 MPa for SA-4 film, which is more than 5 times higher than that of the SA-1 film, owing to the rigid structure including highly oriented crystals and RAF. Meanwhile, SA-4 film features good ductility with an elongation at break of 66%. Moreover, the oriented PGA crystals endow the SA films with excellent heat resistance and dimensional stability. The cost-effective method proposed in this work paves the way for possible large-scale preparation of high-performance PGA films and wider range of applications for PGA materials.

Conflict of Interests

The authors declare no interest conflict.

https://doi.org/10.1007/s10118-023-2894-6

Electronic Supplementary Information

Electronic supplementary information (ESI) is available free of charge in the online version of this article at http://doi.org/10.1007/s10118-023-2894-6.

ACKNOWLEDGMENTS

This work was financially supported by the National Natural Science Foundation of China (Nos. 52073123, 51873082 and 52103032), the Distinguished Young Natural Science Foundation of Jiangsu Province (No. BK20200027) and the Natural Science Foundation of Jiangsu Province (No. BK20200606).

REFERENCES

1 Geyer, R.; Jambeck, J. R.; Law, K. L. Production, use, and fate of all plastics ever made. *Sci. Adv.* **2017**, *3*, 25–29.

2 Wang, Z.; Ganewatta, M. S.; Tang, C. Sustainable polymers from biomass: bridging chemistry with materials and processing. *Prog. Polym. Sci.* **2020**, *101*, 101197.

3 Wang, Q.; Xu, Y.; Xu, P.; Yang, W.; Chen, M.; Dong, W.; Ma, P. Crystallization of microbial polyhydroxyalkanoates: a review. *Int. J. Biol. Macromol.* **2022**, *209*, 330–343.

4 Zeng, Y.; Yang, W.; Xu, P.; Ma, P. A water-resistance soy protein-based adhesive for various substrates application by incorporating tailor-made hydrophobic nanocrystalline cellulose. *Compos. Commun.* **2022**, *32*, 101151.

5 Xu, J. Z.; Li, Y.; Li, Y. K.; Chen, Y. W.; Wang, R.; Liu, G.; Liu, S. M.; Ni, H. W.; Li, Z. M. Shear-induced stereocomplex cylindrites in polylactic acid racemic blends: morphology control and interfacial performance. *Polymer* **2018**, *140*, 179–187.

6 Li, J. X.; Niu, D. Y.; Xu, P. W.; Sun, Z. Y.; Yang, W. J.; Ji, Y.; Ma, P. M. Tailoring the crystallization behavior and mechanical property of poly(glycolic acid) by self-nucleation. *Chinese J. Polym. Sci.* **2022**, *40*, 365–372.

7 Lee, S.; Hongo, C.; Nishino, T. Crystal modulus of poly(glycolic acid) and its temperature dependence. *Macromolecules* **2017**, *50*, 5074–5079.

8 Samantaray, P. K.; Little, A.; Haddleton, D. M.; McNally, T.; Tan, B.; Sun, Z.; Huang, W.; Ji, Y.; Wan, C. Poly(glycolic acid) (PGA): a versatile building block expanding high performance and sustainable bioplastic applications. *Green Chem.* **2020**, *22*, 4055–4081.

9 Yu, C.; Bao, J.; Xie, Q.; Shan, G.; Bao, Y.; Pan, P. Crystallization behavior and crystalline structural changes of poly(glycolic acid) investigated: *via* temperature-variable WAXD and FTIR analysis. *CrystEngComm* **2016**, *18*, 7894–7902.

10 Lee, S. H.; Kim, B. S.; Kim, S. H.; Choi, S. W.; Jeong, S. I.; Kwon, I. K.; Kang, S. W.; Nikolovski, J.; Mooney, D. J.; Han, Y. K.; Kim, Y. H. Elastic biodegradable poly(glycolide-*co*-caprolactone) scaffold for tissue engineering. *J. Biomed. Mater. Res. Part A* **2003**, *66*, 29–37.

11 Li, J.; Rothstein, S. N.; Little, S. R.; Edenborn, H. M.; Meyer, T. Y. The effect of monomer order on the hydrolysis of biodegradable poly(lactic-*co*-glycolic acid) repeating sequence copolymers. *J. Am. Chem. Soc.* **2012**, *134*, 16352–16359.

12 Ding, Y.; Feng, W.; Lu, B.; Wang, P.; Wang, G.; Ji, J. PLA-PEG-PLA tri-block copolymers: effective compatibilizers for promotion of the interfacial structure and mechanical properties of PLA/PBAT blends. *Polymer* **2018**, *146*, 179–187.

13 Qu, Y.; Chen, Y.; Ling, X.; Wu, J.; Hong, J.; Wang, H.; Li, Y. Reactive micro-crosslinked elastomer for supertoughened polylactide. *Macromolecules* **2022**, *55*, 7711–7723.

14 Yang, W.; Qi, G.; Ding, H.; Xu, P.; Dong, W.; Zhu, X.; Zheng, T.; Ma, P. Biodegradable poly(lactic acid)-poly(ε-caprolactone)-nano-lignin composite films with excellent flexibility and UV barrier performance. *Compos. Commun.* **2020**, *22*, 100497.

15 Wu, B.; Zeng, Q.; Niu, D.; Yang, W.; Dong, W.; Chen, M.; Ma, P. Design of supertoughened and heat-resistant PLLA/elastomer blends by controlling the distribution of stereocomplex crystallites and the morphology. *Macromolecules* **2019**, *52*, 1092–1103.

16 Bai, T.; Zhu, B.; Liu, H.; Wang, Y.; Song, G.; Liu, C.; Shen, C. Biodegradable poly(lactic acid) nanocomposites reinforced and toughened by carbon nanotubes/clay hybrids. *Int. J. Biol. Macromol.* **2020**, *151*, 628–634.

17 Samantaray, P. K.; Ellingford, C.; Farris, S.; O'Sullivan, D.; Tan, B.; Sun, Z.; McNally, T.; Wan, C. Electron beam-mediated cross-linking of blown film-extruded biodegradable PGA/PBAT blends toward high toughness and low oxygen permeation. *ACS Sustain. Chem. Eng.* **2022**, *10*, 1267–1276.

18 Wang, R.; Sun, X.; Chen, L.; Liang, W. Morphological and mechanical properties of biodegradable poly(glycolic acid)/poly(butylene adipate-*co*-terephthalate) blends with *in situ* compatibilization. *RSC Adv.* **2021**, *11*, 1241–1249.

19 Niu, D.; Xu, P.; Sun, Z.; Yang, W.; Dong, W.; Ji, Y.; Liu, T.; Du, M.; Lemstra, P. J.; Ma, P. Superior toughened bio-compostable poly(glycolic acid)-based blends with enhanced melt strength *via* selective interfacial localization of *in-situ* grafted copolymers. *Polymer* **2021**, *235*, 124269.

20 Yang, F.; Zhang, C.; Ma, Z.; Weng, Y. *In situ* formation of microfibrillar PBAT in PGA films: an effective way to robust barrier and mechanical properties for fully biodegradable packaging films. *ACS Omega* **2022**, *7*, 21280–21290.

21 Xu, P.; Tan, S.; Niu, D.; Yang, W.; Ma, P. Highly toughened sustainable green polyglycolic acid/polycaprolactone blends with balanced strength: morphology evolution, interfacial compatibilization, and mechanism. *ACS Appl. Polym, Mater.* **2022**. https://doi.org/10.1021/acsapm.2c00715.

22 Cheng, S.; Johnson, L.; Wang, S. Q. Crazing and strain localization of polycarbonate glass in creep. *Polymer* **2013**, *54*, 3363–3369.

23 Zeng, Y.; Yang, Q. C.; Xu, Y. Te; Ma, G. Q.; Huang, H. D.; Lei, J.; Zhong, G. J.; Li, Z. M. Durably ductile, transparent polystyrene based on extensional stress-induced rejuvenation stabilized by styrene-butadiene block copolymer nanofibrils. *ACS Macro Lett.* **2021**, *10*, 71–77.

24 Zeng, Y.; Xu, Y. Te; Zhang, J.; Xu, L.; Ji, X.; Lin, H.; Zhong, G. J.; Li, Z. M. Coupling effect of mechanical and thermal rejuvenation for polystyrene: toward high performance of stiffness, ductility, and transparency. *Macromolecules* **2021**, *54*, 8875–8885.

25 Science, F.; Works, C. The use of a mathematical model to describe isothermal stress-strain curves in glassy thermoplastics. *Proc. R. Soc. London. Ser. A. Math. Phys. Sci.* **1968**, *302*, 453–472.

26 Kargarzadeh, H.; Mariano, M.; Huang, J.; Lin, N.; Ahmad, I.; Dufresne, A.; Thomas, S. Recent developments on nanocellulose reinforced polymer nanocomposites: a review. *Polymer* **2017**, *132*, 368–393.

27 Zhao, Y.; Liu, J.; Li, X.; Lu, Y.; Wang, S. Q. How and why polymer glasses lose their ductility due to plasticizers. *Macromolecules* **2017**, *50*, 2024–2032.

28 Liu, Z.; Li, X.; Zheng, Y.; Wang, S. Q.; Tsige, M. Chain network: key to the ductile behavior of polymer glasses. *Macromolecules* **2018**, *51*, 1666–1673.

29 Wach, R. A.; Wolszczak, P.; Adamus-Wlodarczyk, A. Enhancement of mechanical properties of FDM-PLA parts *via* thermal annealing. *Macromol. Mater. Eng.* **2018**, *303*, 1800169.

30 Huang, T.; Miura, M.; Nobukawa, S.; Yamaguchi, M. Chain packing and its anomalous effect on mechanical toughness for poly(lactic acid). *Biomacromolecules* **2015**, *16*, 1660–1666.
31 Zhou, J.; Zheng, Y.; Shan, G.; Bao, Y.; Wang, W. J.; Pan, P. Stretch-induced crystalline structural evolution and cavitation of poly(butylene adipate-*ran*-butylene terephthalate)/poly(lactic acid) immiscible blends. *Polymer* **2020**, *188*, 122121.
32 Gao, X. R.; Li, Y.; Huang, H. D.; Xu, J. Z.; Xu, L.; Ji, X.; Zhong, G. J.; Li, Z. M. Extensional stress-induced orientation and crystallization can regulate the balance of toughness and stiffness of polylactide films: interplay of oriented amorphous chains and crystallites. *Macromolecules* **2019**, *52*, 5278–5288.
33 Razavi, M.; Wang, S. Q. Why is crystalline poly(lactic acid) brittle at room temperature. *Macromolecules* **2019**, *52*, 5429–5441.
34 Xu, P. P.; Yang, S.; Gao, X. R.; Chen, S. P.; Xu, L.; Zhong, G. J.; Huang, H. D.; Li, Z. M. Constructing robust chain entanglement network, well-defined nanosized crystals and highly aligned graphene oxide nanosheets: towards strong, ductile and high barrier poly(lactic acid) nanocomposite films for green packaging. *Compos. Part B Eng.* **2021**, *222*, 109048.
35 Zhou, L.; Xu, P. P.; Ni, S. H.; Xu, L.; Lin, H.; Zhong, G. J.; Huang, H. D.; Li, Z. M. Superior ductile and high-barrier poly(lactic acid) films by constructing oriented nanocrystals as efficient reinforcement of chain entanglement network and promising barrier wall. *Chinese J. Polym. Sci.* **2022**, *40*, 1201–1212.
36 Yang, S.; Luo, C.; Lin, H.; Xu, P. P.; Xu, L.; Lei, J.; Zhong, G. J.; Li, Z. M. Robust propylene-ethylene copolymer/polypropylene films: extensional stress-induced orientation realized at low temperature processing. *Polymer* **2020**, *206*, 122848.
37 Li, J.; Niu, D.; Liu, B.; Xu, P.; Yang, W.; Jan, P.; Ma, P. Improvement on the mechanical performance and resistance towards hydrolysis of poly(glycolic acid) *via* solid-state drawing. *Chinese J. Polym. Sci.* **2023**, *41*, 14–23.
38 Wang, Z.; Ma, Z.; Li, L. Flow-induced crystallization of polymers: molecular and thermodynamic considerations. *Macromolecules* **2016**, *49*, 1505–1517.
39 Montes de Oca, H.; Ward, I. M. Structure and mechanical properties of PGA crystals and fibres. *Polymer* **2006**, *47*, 7070–7077.
40 Lei, C.; Xu, R.; Tian, Z.; Huang, H.; Xie, J.; Zhu, X. Stretching-induced uniform micropores formation: an *in situ* SAXS/WAXS study. *Macromolecules* **2018**, *51*, 3433–3442.
41 Cui, K.; Ma, Z.; Wang, Z.; Ji, Y.; Liu, D.; Huang, N.; Chen, L.; Zhang, W.; Li, L. Kinetic process of shish formation: from stretched network to stabilized nuclei. *Macromolecules* **2015**, *48*, 5276–5285.
42 Lan, Q.; Li, Y.; Chi, H. Highly enhanced mesophase formation in glassy poly(l-lactide) at low temperatures by low-pressure CO_2 that provides moderately increased molecular mobility. *Macromolecules* **2016**, *49*, 2262–2271.
43 Stoclet, G.; Seguela, R.; Lefebvre, J. M.; Rochas, C. New insights on the strain-induced mesophase of poly(D,L-lactide): *in situ* WAXS and DSC study of the thermo-mechanical stability. *Macromolecules* **2010**, *43*, 7228–7237.
44 Lee, S.; Han, J.; Jeong, Y.; Kwon, M. Strain-induced enthalpy relaxation in poly(lactic acid). *Macromolecules* **2010**, *43*, 25–28.
45 Delpouve, N.; Delbreilh, L.; Stoclet, G.; Saiter, A.; Dargent, E. Structural dependence of the molecular mobility in the amorphous fractions of polylactide. *Macromolecules* **2014**, *47*, 5186–5197.
46 Ma, J.; Yu, L.; Chen, S.; Chen, W.; Wang, Y.; Guang, S.; Zhang, X.; Lu, W.; Wang, Y.; Bao, J. Structure-property evolution of poly(ethylene terephthalate) fibers in industrialized process under complex coupling of stress and temperature field. *Macromolecules* **2019**, *52*, 565–574.
47 Wang, Y.; Ribelles, J. L. G.; Sánchez, M. S.; Mano, J. F. Morphological contributions to glass transition in poly(L-lactic acid). *Macromolecules* **2005**, *38*, 4712–4718.
48 Cowie, J. M. G.; Arrighi, V. Physical aging of polymer blends. *Polym. Blends Handb.* **2014**, *20*, 1357–1394.
49 Zhao, J.; Wang, J.; Li, C.; Fan, Q. Study of the amorphous phase in semicrystalline poly(ethylene terephthalate) *via* physical aging. *Macromolecules* **2002**, *35*, 3097–3103.

https://doi.org/10.1007/s10118-023-2894-6